Letter

Quantum geometric bound and ideal condition for Euler band topology

Soonhyun Kwon [1,2] and Bohm-Jung Yang [1,2,3,4,*]

[1]*Department of Physics and Astronomy, Seoul National University, Seoul 08826, Korea*
[2]*Center for Theoretical Physics (CTP), Seoul National University, Seoul 08826, Korea*
[3]*Center for Correlated Electron Systems, Institute for Basic Science (IBS), Seoul 08826, Korea*
[4]*Institute of Applied Physics, Seoul National University, Seoul 08826, Korea*

(Received 28 November 2023; revised 13 March 2024; accepted 29 March 2024; published 22 April 2024)

Understanding the relationship between quantum geometry and topological invariants is a central problem in the study of topological states. In this work, we establish the relationship between the quantum metric and the Euler curvature in two-dimensional systems with space-time inversion I_{ST} symmetry satisfying $I_{ST}^2 = +1$. As I_{ST} symmetry imposes the reality of the wave function with vanishing Berry curvature, the well-known inequality between the quantum metric and the Berry curvature is not meaningful in this class of systems. We find that the non-Abelian quantum geometric tensor of two real bands exhibits an intriguing inequality between the off-diagonal Berry curvature and the quantum metric, which in turn gives the inequality between the quantum volume and the Euler invariant. Moreover, we show that the saturation condition of the inequality is deeply related to the ideal condition for Euler bands, which provides a criterion for the stability of fractional topological phases in interacting Euler bands. Our findings demonstrate the potential of the quantum geometry as a powerful tool for characterizing symmetry-protected topological states and their interaction effect.

DOI: 10.1103/PhysRevB.109.L161111

Introduction. The geometry of quantum states is characterized by the quantum geometric tensor (QGT) whose symmetric real and antisymmetric imaginary parts correspond to the quantum metric (QM) and Berry curvature (BC), respectively. The integral of local geometric quantities such as QM and BC often gives information about the global topology [1–11]. A well-known example is the first Chern number that is given by the integral of the BC over a closed two-dimensional (2D) space. The first Chern number governs the topological properties of 2D insulators in the absence of symmetry constraints [1–9], which clearly demonstrates the intimate relationship between the geometry and topology of quantum states.

Not only the BC, but the QM also carries information about global topology. For instance, the quantum volume, the volume of the parameter space measured by the QM, has a lower bound determined by the first Chern number [10,12–15]. However, when the system is under certain symmetry constraints, its global topology is not necessarily characterized by the first Chern number as shown in various symmetry-protected topological states, while the definition of the quantum volumes remains the same [16–19]. Therefore, it remains a question whether symmetry-protected topology can give a bound of the quantum volume or even be related to it. In particular, when symmetry constraints force the BC to be strictly zero, revealing the relationship of the quantum volume to global topology is an intriguing open question.

In fact, the relation between the quantum volume and the Chern number arises from the fundamental local inequality between the QM and BC. In particular, when the local inequality saturates, the corresponding Chern band is expected to host fractional Chern insulators when an interaction effect is included [20–23]. Thus, extending the fundamental local inequality between the QM and BC to systems with vanishing BC is an important step towards the complete understanding of many-body instabilities in interacting symmetry-protected topological bands.

In this Letter, we establish the relationship between the quantum metric and Euler band topology in 2D systems with space-time inversion I_{ST} symmetry. When the antiunitary I_{ST} symmetry satisfying $I_{ST}^2 = 1$ exists, there is a basis in which the Bloch Hamiltonian and the relevant wave functions become real. Thus, the BC vanishes at every momentum and the first Chern number is always zero. However, interestingly, two isolated bands in I_{ST} symmetric systems carry another integer $\mathbb{Z}$ topological invariant, called the Euler number e_2 [24–28]. Here, we derive the fundamental local inequality between the QM and Euler curvature. Based on this, we establish the relation between the quantum volume and the Euler number. Moreover, from the saturation condition of the local inequality, we derive the ideal condition for topological Euler bands, and demonstrate the band geometric criterion on the correlation effect in interacting Euler bands. Considering the recent discovery of the Euler band topology in the nearly flat bands of twisted bilayer graphene (TBG) at magic angles, our theory will shed light on their fascinating correlated topological properties [29–34].

Quantum geometry of Chern bands. Generally, the non-Abelian QGT is given by

$$Q_{\mu\nu}^{ij}(\mathbf{k}) = \langle \partial_\mu u_i(\mathbf{k}) | \left[1 - P(\mathbf{k})\right] | \partial_\nu u_j(\mathbf{k}) \rangle \,, \tag{1}$$

*bjyang@snu.ac.kr

where $\mu, \nu = x, y, z$ denote spatial coordinates, $\partial_\mu = \partial/\partial k_\mu$, and $P(\mathbf{k}) = \sum_{i=1}^{N} |u_i(\mathbf{k})\rangle \langle u_i(\mathbf{k})|$ indicates the projection operator to the space spanned by the states $\{|u_{1,\ldots,N}(\mathbf{k})\rangle\}$ [35–42]. The quantum metric $g_{\mu\nu}(\mathbf{k}) \equiv \frac{1}{2}\mathrm{Tr}[Q_{\mu\nu} + Q_{\nu\mu}]$ and the Berry curvature $\Omega_{\mu\nu}(\mathbf{k}) \equiv i\mathrm{Tr}[Q_{\mu\nu} - Q_{\nu\mu}]$ with the trace over band indices are generally invariant under $U(N)$ gauge transformation for complex wave functions.

The BC $\Omega^n(\mathbf{k})$ and QM $g^n_{ij}(\mathbf{k})$ of a band with index n satisfy the following inequality [15],

$$\sqrt{\det\left[g^n_{\mu\nu}(\mathbf{k})\right]} \geqslant \tfrac{1}{2}|\Omega^n(\mathbf{k})|, \tag{2}$$

whose physical significance can be understand in the following context. First, when both sides of the inequality are integrated over the 2D Brillouin zone (BZ), we obtain the relation $\mathrm{vol}_g \geqslant \pi|C|$, where C is the Chern number and vol_g is the quantum volume defined as $\mathrm{vol}_g \equiv \int d^2\mathbf{k}\sqrt{\det[g^n_{\mu\nu}(\mathbf{k})]}$, which is the volume of the parameter space computed using QM as the metric. vol_g is an excellent measure of the Chern band topology in many systems including Landau levels and two-band Hamiltonians where the equality $\mathrm{vol}_g = \pi|C|$ holds as well as the flat band systems where $\mathrm{vol}_g \approx \pi|C|$ [15].

Second, the saturation of the inequality in Eq. (2) provides an important criterion to achieve fractional topological phases in interacting Chern bands [43–45]. The saturation of the inequality with nonzero BC means that the QGT $Q^n_{\mu\nu}(\mathbf{k}) = g^n_{\mu\nu}(\mathbf{k}) - i\frac{1}{2}\epsilon_{\mu\nu}\Omega^n(\mathbf{k})$ has a null vector, which in turn gives the relation $g^n_{\mu\nu}(\mathbf{k}) = \frac{1}{2}\Omega^n(\mathbf{k})\omega_{\mu\nu}(\mathbf{k})$ where $\omega_{\mu\nu}(\mathbf{k})$ is a $\mathbf{k}$-dependent symmetric matrix with unit determinant [46] (see the Supplemental Material (SM) [47]). To mimic the lowest Landau level (LLL) under uniform magnetic field, we further assume $\mathbf{k}$ independence of $\omega_{\mu\nu}(\mathbf{k})$ leading to the following *ideal condition* for Chern bands,

$$g^n_{\mu\nu}(\mathbf{k}) = \tfrac{1}{2}\Omega^n(\mathbf{k})\omega_{\mu\nu}, \tag{3}$$

where $\omega_{\mu\nu}$ is a constant symmetric matrix with unit determinant [46,48]. If Eq. (3) is satisfied, the equality in Eq. (2) also holds. According to [46,49], the Bloch wave function $|u(\mathbf{k})\rangle$ of an ideal Chern band can be decomposed, like LLL wave functions, as

$$|u(\mathbf{k})\rangle = \frac{1}{N_\mathbf{k}}|\tilde{u}(k)\rangle, \tag{4}$$

where $|\tilde{u}(k)\rangle$ is a holomorphic function of a complex number $k \equiv \lambda_x\mathbf{k}_x + \lambda_y\mathbf{k}_x$ and $N_\mathbf{k}$ is the normalization factor. The complex numbers $\lambda_{x,y}$ satisfy $\omega_{\mu\nu} = \lambda^*_x\lambda_y + \lambda_x\lambda^*_y$ and $i\epsilon_{\mu\nu} = \lambda^*_\mu\lambda_\nu - \lambda_\mu\lambda^*_\nu$ where $\epsilon_{\mu\nu}$ is a fully antisymmetric tensor.

Moreover, when the BC of an ideal Chern band is constant, the corresponding projected density operator $\bar{\rho}_n(\mathbf{k}) = P_n e^{i\mathbf{k}\cdot\mathbf{r}}P_n$ where $P_n = \int |u_n(\mathbf{k})\rangle\langle u_n(\mathbf{k})|\, d\mathbf{k}$ satisfies the so-called Girvin-MacDonald-Platzman (GMP) algebra,

$$[\bar{\rho}_n(\mathbf{k}), \bar{\rho}_n(\mathbf{q})] = 2ie^{\mathbf{k}_\mu g^n_{\mu\nu}\mathbf{q}_\nu}\sin\left[\left(\mathbf{k}_x\mathbf{q}_y - \mathbf{k}_y\mathbf{q}_x\right)\Omega^n_{xy}\right]\bar{\rho}_n(\mathbf{k}+\mathbf{q}), \tag{5}$$

as in LLL [50,51], which indicates the stability of the many-body ground state with fractional topology [43–45,50,51]. Interestingly, recent numerical studies have shown that what is essential to achieve the fractional Chern band is not the constant BC but the ideal condition in Eq. (3) [43,46].

Non-Abelian quantum geometry of two real bands. In two dimensions, I_{ST} symmetry appears in the form of $I_{ST} = PT$ with time-reversal T and inversion P symmetries in spinless fermion systems, or $I_{ST} = C_{2z}T$ with twofold rotation C_{2z} symmetry about the z axis in both spinless and spinful fermion systems. As the antiunitary I_{ST} symmetry is local in momentum space and satisfies $I^2_{ST} = 1$, it can be represented by $I_{ST} = K$ with the complex conjugation operator K. Then, the I_{ST} symmetry of the wave function $|u_i(\mathbf{k})\rangle$ (i is a band index) imposes the reality condition $I_{ST}|u_i(\mathbf{k})\rangle = |u_i(\mathbf{k})\rangle^* = |u_i(\mathbf{k})\rangle$, which forces the Berry curvature to vanish at every momentum $\mathbf{k}$. Thus, the Chern number of I_{ST} symmetric systems is always zero. However, two real bands can have nontrivial band topology characterized by the integer Euler invariant as explained below.

For two real bands $|u_{1,2}(\mathbf{k})\rangle$, the invariance of the non-Abelian QGT under $O(2)$ gauge transformation leaves $g_{\mu\nu}(\mathbf{k}) = Q^{11}_{\mu\nu}(\mathbf{k}) + Q^{22}_{\mu\nu}(\mathbf{k})$ as the only gauge-invariant combination. On the other hand, under $SO(2)$ gauge transformation that preserves the orientation of two real bands, one can find another gauge-invariant linear combination $Q^{12}_{\mu\nu}(\mathbf{k}) - Q^{21}_{\mu\nu}(\mathbf{k})$, which gives the off-diagonal Berry curvature $F_{12}(\mathbf{k}) \equiv Q^{12}_{xy}(\mathbf{k}) - Q^{21}_{yx}(\mathbf{k}) = \nabla \times \langle u_1(\mathbf{k})|\nabla|u_2(\mathbf{k})\rangle$. When the orientation of two real bands is fixed, the integral of $F_{12}(\mathbf{k})$ becomes the Euler invariant

$$e_2 = \frac{1}{2\pi}\int_{BZ} d^2\mathbf{k}F_{12}(\mathbf{k}), \tag{6}$$

which classifies the topology of orientable real two bands [24–28]. For real bands $|u_{1,2}(\mathbf{k})\rangle$, one can find a Chern basis $|u_\pm(\mathbf{k})\rangle = \frac{1}{\sqrt{2}}[|u_1(\mathbf{k})\rangle \pm i|u_2(\mathbf{k})\rangle]$ satisfying that when $|u_{1,2}(\mathbf{k})\rangle$ have the Euler number e_2, $|u_\pm(\mathbf{k})\rangle$ have the Chern numbers $\pm e_2$, respectively.

Quantum volume and topology of Euler bands. The local geometric quantities $g_{\mu\nu}(\mathbf{k})$ and $F_{12}(\mathbf{k})$ of two real bands $|u_{1,2}(\mathbf{k})\rangle$ satisfy the inequality

$$\sqrt{\det[g_{\mu\nu}(\mathbf{k})]} \geqslant |F_{12}(\mathbf{k})|, \tag{7}$$

which gives tighter bounds than in previous works [30,52,53] as shown in SM [47]. By integrating both sides over 2D BZ, we obtain

$$\mathrm{vol}_g \geqslant \int d^2\mathbf{k}|F_{12}(\mathbf{k})| \geqslant \left|\int d^2\mathbf{k}F_{12}(\mathbf{k})\right| \geqslant 2\pi|e_2|. \tag{8}$$

As a direct consequence of this inequality, if $\mathrm{vol}_g < 2\pi$, then $|e_2| = 0$; i.e., two isolated real bands are topologically trivial. In systems with $\mathrm{vol}_g \geqslant 2\pi$, the inequality does not give definite information about topology. However, as shown below with several examples, $\mathrm{vol}_g/2\pi$ often gives an excellent estimate of topology and approaches the Euler number from above in a proper limit.

Three-band models. Let us illustrate the relationship between the Euler topology and quantum volume by constructing minimal model Hamiltonians. Since two real bands with nonzero Euler invariant have fragile Wannier obstruction [54–59], the minimal lattice model for an Euler insulator

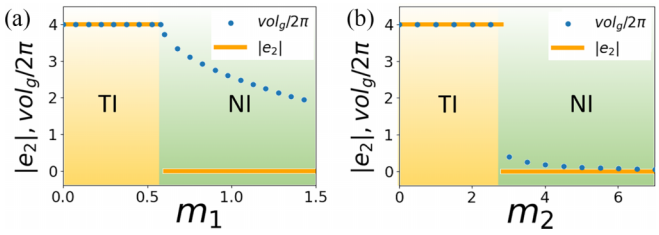

FIG. 1. (a), (b) The change of the quantum volume and Euler invariant of the lower two flat bands for three-band models where a direct transition between a topological insulator (TI) with $e_2 \neq 0$ and a normal insulator (NI) with $e_2 = 0$ occurs.

should have at least three bands with two Euler bands (bands 1 and 2) decoupled from the third band (band 3).

In general, such three-band models have two special properties. First, there must be a point in the BZ where $\det[g_{\mu\nu}(\mathbf{k})] = |F_{12}(\mathbf{k})| = 0$ for two Euler bands as proved in SM [47]. As a consequence, neither $g_{\mu\nu}(\mathbf{k})$ nor $F_{12}(\mathbf{k})$ can be nonzero while remaining uniform in the BZ. Second, the equality $\sqrt{\det[g_{\mu\nu}(\mathbf{k})]} = |F_{12}(\mathbf{k})|$ always holds as shown in SM [47]. A simple consequence is that, if F_{12} has the same sign over the entire BZ, $\mathrm{vol}_g = 2\pi\,|e_2|$. In this case, the quantum volume directly measures e_2.

A three-band model possessing two bands with $e_2 \neq 0$ can be constructed by using a two-band Chern insulator model

$$H_{\mathrm{Chern}}(\mathbf{k}) = a(\mathbf{k})\sigma_x + b(\mathbf{k})\sigma_y + c(\mathbf{k})\sigma_z, \tag{9}$$

where $a(\mathbf{k})$, $b(\mathbf{k})$, $c(\mathbf{k})$ are real functions and $\sigma_{x,y,z}$ are Pauli matrices. The corresponding real three-band model is given by

$$H_{\mathrm{Euler}}(\mathbf{k}) = \begin{pmatrix} a(\mathbf{k})^2 & a(\mathbf{k})b(\mathbf{k}) & a(\mathbf{k})c(\mathbf{k}) \\ a(\mathbf{k})b(\mathbf{k}) & b(\mathbf{k})^2 & b(\mathbf{k})c(\mathbf{k}) \\ a(\mathbf{k})c(\mathbf{k}) & b(\mathbf{k})c(\mathbf{k}) & c(\mathbf{k})^2 \end{pmatrix}, \tag{10}$$

which has two degenerate flat bands at zero energy and a dispersive band with energy $a(\mathbf{k})^2 + b(\mathbf{k})^2 + c(\mathbf{k})^2$. The BC $\Omega(\mathbf{k})$ of Eq. (9) and the off-diagonal BC $F_{12}(\mathbf{k})$ of the two flat bands of Eq. (10) satisfy

$$|F_{12}(\mathbf{k})| = 2|\Omega(\mathbf{k})|, \tag{11}$$

as proved in SM [47]. Let us note that regardless of the band dispersion of the Chern insulator, the resulting two Euler bands are perfectly flat.

For example, let us consider a variant of the square lattice Chern insulator model introduced in [60] with $a(\mathbf{k}) = (2 - \sqrt{2})t\sin(k_x)\sin(k_y) - m_2$, $b(\mathbf{k}) = \sqrt{2}t[\cos(k_y) + \cos(k_x)] - m_1$, $c(\mathbf{k}) = \sqrt{2}t[\cos(k_y) - \cos(k_x)]$. When $m_2 = 0$, the Chern number of the lower band is -2 (0) when $|m_1| < 2\sqrt{2}|t|$ ($|m_1| > 2\sqrt{2}|t|$). Accordingly, two degenerate flat bands of the corresponding three-band model have $e_2 = 4$ ($e_2 = 0$) when $|m_1| < 2\sqrt{2}|t|$ ($|m_1| > 2\sqrt{2}|t|$). The change of $\mathrm{vol}_g/2\pi$ and e_2 as a function of m_1 is plotted in Fig. 1(a). Figure 1(b) is a similar plot when m_2 is varied with $m_1 = 0$. In both cases, $\mathrm{vol}_g/2\pi$ is an excellent approximation of e_2 when $e_2 \neq 0$. But depending on which parameter is changed, the quantum volume can change either continuously or discontinuously.

We note that when the degeneracy of the two flat Euler bands is lifted, a topological phase transition changing e_2 is mediated by an intermediate semimetal phase [24]. Interestingly, although e_2 is not well defined in the gapless region, when gap closing points have linear dispersion, the quantum volume is finite and changes smoothly even in the gapless region, as shown in SM [47].

Multiband models. Here, we propose a general way to construct a $2N$-band model with two Euler bands decoupled from other bands by superposing two N-band Hamiltonians with an isolated Chern band (N is an integer). One advantage of this construction is that the well-established inequality in Eq. (2) and its saturation condition for a Chern band [15] naturally extend to similar relations for Euler bands.

Explicitly, let us superpose an N-band Hamiltonian $H_{\mathrm{Chern}}(\mathbf{k})$ having an isolated Chern band with its complex conjugate as

$$H_{\mathrm{Euler}}(\mathbf{k}) = \begin{pmatrix} H_{\mathrm{Chern}}(\mathbf{k}) & 0 \\ 0 & H^*_{\mathrm{Chern}}(\mathbf{k}) \end{pmatrix}. \tag{12}$$

Then, each band of H_{Euler} is doubly degenerate, and the Chern band of $H_{\mathrm{Chern}}(\mathbf{k})$ turns into degenerate Euler bands of H_{Euler}. After a unitary transformation described in SM [47], $H_{\mathrm{Euler}}(\mathbf{k})$ can become real and commute with a matrix τ_y as

$$\tilde{H}_{\mathrm{Euler}}(\mathbf{k}) = \mathrm{Re}[H_{\mathrm{Chern}}(\mathbf{k})] \otimes \tau_0 - \mathrm{Im}[H_{\mathrm{Chern}}(\mathbf{k})] \otimes i\tau_y, \tag{13}$$

where $\tau_{x,y,z}$ are Pauli matrices connecting two N-band Hamiltonians and τ_0 is the relevant 2×2 identity matrix.

The BC $\Omega(\mathbf{k})$ and QM $g^{\mathrm{Chern}}_{ij}(\mathbf{k})$ of the Chern band in H_{Chern} and the Euler curvature $F_{12}(\mathbf{k})$ and QM $g^{\mathrm{Euler}}_{ij}(\mathbf{k})$ of the Euler bands in $\tilde{H}_{\mathrm{Euler}}(\mathbf{k})$ satisfy the following relation,

$$\begin{aligned} |F_{12}(\mathbf{k})| &= |\Omega(\mathbf{k})|, \\ \sqrt{\det\left[g^{\mathrm{Euler}}_{ij}(\mathbf{k})\right]} &= 2\sqrt{\det\left[g^{\mathrm{Chern}}_{ij}(\mathbf{k})\right]}, \end{aligned} \tag{14}$$

as proved in SM [47]. This clearly demonstrates that the band topology of the mapped Euler bands can be well approximated by the quantum volume in the same manner as the Chern band case.

For example, let us construct a four-band model which can be mapped to two superposed two-band Chern insulators in certain limits. In such limits, as the inequality in Eq. (2) becomes the equality for two-band Chern insulators, a similar equality should hold for Euler bands. Explicitly, we consider the Hamiltonian $H^a_4(\mathbf{k})$ with components $H^a_4(\mathbf{k}) = a(\mathbf{k})\sigma_x + b(\mathbf{k})\tau_y \otimes \sigma_y + c(\mathbf{k})\sigma_z + m_3\tau_x \otimes \sigma_x$ where $\sigma_{x,y,z,}$, $\tau_{x,y,z}$ are Pauli matrices, and $a(\mathbf{k})$, $b(\mathbf{k})$, $c(\mathbf{k})$ are the same as those in the previous three-band model with $t = 1$ and $m_1 = m_2 = 0$. The band dispersion at $m_3 = 0$ is shown in Fig. 2(a). When $m_3 = 0$, the Hamiltonian commutes with τ_y, and thus can be written as in Eq. (13). As shown in Fig. 2(c), $\mathrm{vol}_g/2\pi$ and $|e_2|$ of lower degenerate bands coincide only at $m_3 = 0$. The same also holds for upper degenerate bands.

When the real Hamiltonian hosting Euler bands has additional chiral S symmetry satisfying $S^2 = 1$ and $[S, I_{ST}] = 0$, two Euler bands can appear as isolated zero-energy flat bands when $\mathrm{Tr}[S] = \pm 2$. Especially, the zero-energy states of a $(2N + 2)$-band real Hamiltonian with chiral symmetry can be considered as those of a related $(N + 2)$-band Hamiltonian sharing the same Euler band topology (see SM [47]). This

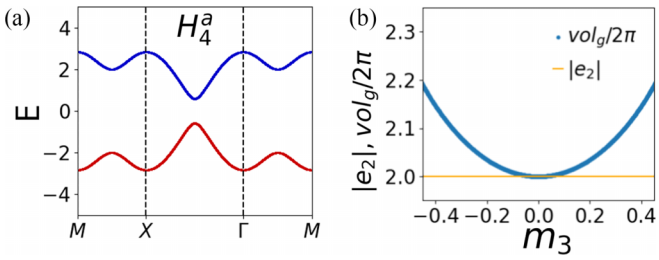

FIG. 2. (a) The band structure of the four-band model $H_4^a(\mathbf{k})$ when $m_3 = 0$. Both red and blue bands are doubly degenerate when $m_3 = 0$ while the degeneracy is lifted when $m_3 \neq 0$. (b) The quantum volume and Euler invariant of the red band in (a).

means that a 4-band chiral symmetric Hamiltonian with zero-energy flat Euler bands, satisfying $\sqrt{\det[g_{\mu\nu}(\mathbf{k})]} = |F_{12}(\mathbf{k})|$ as in 3-band models, can also be constructed.

On the other hand, if $\{S, I_{ST}\} = 0$ is satisfied, two isolated bands cannot have $e_2 \neq 0$ in periodic real Hamiltonians as shown in SM [47]. One exception is when Euler bands appear as effective low-energy bands of quasiperiodic systems as in TBG discussed below.

Ideal Euler bands and correlation effect. Here, we address the question of possible fractional topological phases in interacting Euler bands from the band-geometric point of view. First, we define *ideal Euler bands* as two real bands $|u_{1,2}(\mathbf{k})\rangle$ whose QGT satisfies

$$g_{\mu\nu}(\mathbf{k}) = F_{12}(\mathbf{k})\omega_{\mu\nu}, \tag{15}$$

which is equivalent to the ideal condition for Chern bands in Eq. (3). Ideal Euler bands always satisfy the equality of Eq. (7). We note that the corresponding Chern basis $|u_\pm(\mathbf{k})\rangle = \frac{1}{\sqrt{2}}[|u_1(\mathbf{k})\rangle \pm i\,|u_2(\mathbf{k})\rangle]$ satisfies the ideal condition in Eq. (3).

Since Eq. (15) is equivalent to the condition that the QGT $G_{\mu\nu}(\mathbf{k}) \equiv g_{\mu\nu}(\mathbf{k}) + i\epsilon_{\mu\nu}F_{12}(\mathbf{k})$ with $F_{12}(\mathbf{k}) \neq 0$ has a constant null vector, the wave function for ideal Euler bands and the corresponding Chern basis can always be written as in Eq. (4), analogous to LLL (see SM [47]). This indicates the potential that fractional topological insulators may appear in partially filled interacting ideal Euler bands [46]. Moreover, when $F_{12}(\mathbf{k})$ of ideal Euler bands is constant in momentum space, the projected density operators $\bar{\rho}_{\alpha\beta}(\mathbf{k}) = P_\alpha e^{i\mathbf{k}\cdot\mathbf{r}}P_\beta$ where $P_\alpha = \int |u_\alpha(\mathbf{k})\rangle\langle u_\alpha(\mathbf{k})|\,d\mathbf{k}$ $(\alpha = \pm)$ for the Chern basis $|u_\pm(\mathbf{k})\rangle$ also satisfy the algebraic relation similar to the GMP algebra when $\alpha = \beta$, which further supports the possible fractional topological phases. However, as $\bar{\rho}_{\alpha\beta}(\mathbf{k})$ with $\alpha \neq \beta$ do not satisfy closed algebraic relations, ideal Euler bands are different from two copies of ideal Chern bands; thus one may expect distinct many-body ground states in interacting Euler bands (see SM [47]).

Unfortunately, both ideal Chern and ideal Euler bands cannot be realized in periodic lattice Hamiltonians where the atomic positions are given by a linear combination of primitive lattice vectors with rational coefficients, which includes most of known lattice systems. This happens because the decomposition in Eq. (4) is not compatible with nonzero Chern or Euler number, as shown in SM [47]. However, ideal bands can be realized in continuum models, as an effective periodic low-energy model of quasiperiodic systems such as TBG.

In general, one can construct a continuum model hosting ideal Euler bands as follows. For given ideal Euler bands $|u_{1,2}(\mathbf{k})\rangle$, the Chern basis $|u_\pm(\mathbf{k})\rangle$ can be written as

$$|u_+(\mathbf{k})\rangle = [|u_-(\mathbf{k})\rangle]^* = \frac{1}{N_\mathbf{k}}|\tilde{u}(k)\rangle\,, \tag{16}$$

where $N_\mathbf{k}$ is the normalizaton factor. The holomorphic function $|\tilde{u}(k)\rangle$ satisfies (i) $[\langle\tilde{u}(k)|]^*\,|\tilde{u}(k)\rangle = 0$ because of the normalization of $|u_{1,2}(\mathbf{k})\rangle$, and (ii) $\forall k$, $\langle\tilde{u}(k)|\,|\tilde{u}(k)\rangle \neq 0$ because of the normalization condition in Eq. (16). Using $|u_+(\mathbf{k})\rangle$ and $|\tilde{u}(k)\rangle$, the Euler curvature and quantum metric of the Euler bands can be calculated as

$$\begin{aligned} F_{12}(\mathbf{k}) &= i(\lambda_y^*\lambda_x - \lambda_x^*\lambda_y)\,\langle v(\mathbf{k})|\,|v(\mathbf{k})\rangle = \langle v(\mathbf{k})|\,|v(\mathbf{k})\rangle\,, \\ g_{\alpha\beta}(\mathbf{k}) &= (\lambda_\alpha^*\lambda_\beta + \lambda_\beta^*\lambda_\alpha)\,\langle v(\mathbf{k})|\,|v(\mathbf{k})\rangle = \omega_{\alpha\beta}\,\langle v(\mathbf{k})|\,|v(\mathbf{k})\rangle\,, \end{aligned} \tag{17}$$

where

$$|v(\mathbf{k})\rangle = \frac{1}{N_\mathbf{k}}[1 - |u_+(\mathbf{k})\rangle\langle u_+(\mathbf{k})|]\,|\partial_k\tilde{u}(k)\rangle\,. \tag{18}$$

In Eq. (17), the ideality of Euler bands manifests.

Now, let us construct a 3-band continuum model hosting ideal Euler bands. Defining $|\tilde{u}(k)\rangle^t = (\tilde{u}_1(k), \tilde{u}_2(k), \tilde{u}_3(k))$, one can choose $\tilde{u}_1(k) = f_1(k)^2 - f_2(k)^2$, $\tilde{u}_2(k) = i[f_1(k)^2 + f_2(k)^2]$, $\tilde{u}_3(k) = 2f_1(k)f_2(k)$ where $f_{1,2}(k)$ are analytic polynomial functions of k. The above choice of $\tilde{u}_1(k)$, $\tilde{u}_2(k)$, $\tilde{u}_3(k)$ satisfies two conditions (i) $[\langle\tilde{u}(k)|]^*\,|\tilde{u}(k)\rangle = 0$ and (ii) $\langle\tilde{u}(k)|\,|\tilde{u}(k)\rangle \neq 0$ for any k. The Hamiltonian $H(\mathbf{k}) = |z(k)\rangle\langle z(k)|$ with

$$|z(k)\rangle = \begin{pmatrix} f_1(k)^*f_2(k) + f_1(k)f_2(k)^* \\ \frac{1}{i}[f_1(k)^*f_2(k) - f_1(k)f_2(k)^*] \\ |f_2(k)|^2 - |f_1(k)|^2 \end{pmatrix} \tag{19}$$

has zero-energy degenerate flat ideal Euler bands and the third band with energy $[|f_1(k)|^2 + |f_2(k)|^2]^2 > 0$. Choosing $f_1(k) = k$, $f_2(k) = 1$, the Euler bands have $e_2 = \pm 2$. See SM for more general discussion [47].

Twisted bilayer graphene. The nearly flat bands at charge neutrality in TBG with small twist angle θ are the representative example of Euler bands with $e_2 = 1$ [24], which can be described by the continuum model H_{BM} proposed by Bistritzer and MacDonald [61]. The low-energy band structure of H_{BM} can be characterized by two dimensionless parameters ω_0/ω_1 and $\alpha = \omega_1/(v_0k_\theta)$ where ω_0 and ω_1 describe the interlayer couplings between AA/BB sites and AB/BA sites, respectively [see Fig. 3(a)] [61]. v_0 is the Fermi velocity of Dirac points and $k_\theta = 8\pi\sin(\theta/2)/3a$ with lattice constant a (see SM [47] for details).

When $\omega_0/\omega_1 = 0$, TBG has chiral symmetry S that anticommutes with $C_{2z}T$. However, the flat bands in TBG can carry nonzero e_2 because of the quasiperiodicity of TBG (see SM [47]). When chiral symmetry exists, $\mathrm{vol}_g/2\pi = e_2 = 1$ holds at each magic angle with flat bands as shown in Fig. 3(b).

When chiral symmetry is broken, $\mathrm{vol}_g/2\pi > e_2$ holds [Fig. 3(c)]. Also, the minimum quantum volume, minimum bandwidth, and minimum Dirac velocity appear at different θ's [Fig. 3(d)], each of which has its own physical

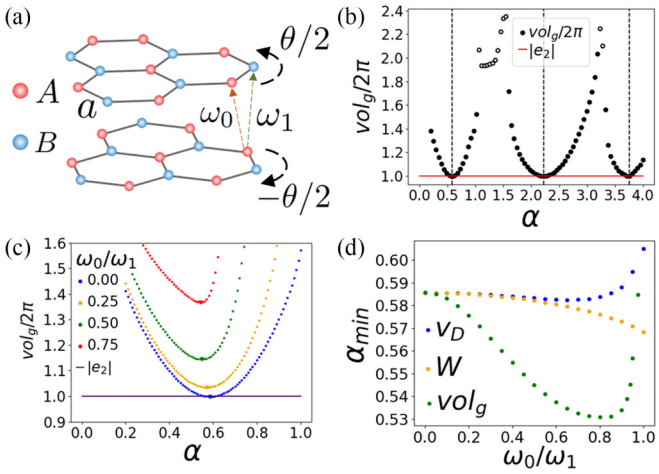

FIG. 3. (a) The lattice structure of TBG with the twist angle θ. (b) The change of the quantum volume and Euler invariant as a function of α at the chiral limit with $\omega_0/\omega_1 = 0$. $\mathrm{vol}_g/2\pi = |e_2|$ holds only at magic angles. (c) Similar plot for different ω_0/ω_1. (d) Plot of α_{min} at which the Dirac velocity v_D, the flat-band bandwidth W, or vol_g becomes minimized at a given ω_0/ω_1 as a function of ω_0/ω_1.

significance. Considering interaction effect, however, θ with minimum quantum volume is special because two quantities on both sides in Eq. (7) are closest at this point, thus correlation-induced fractional topological phases should be the most favorable around it.

Discussion. In the case of TBG in the chiral limit, because chiral symmetry satisfies $S^2 = 1$, $\{S, I_{ST}\} = 0$, the ideal Euler bands at magic angle are reduced to two decoupled ideal Chern bands on which most of the recent theoretical studies on correlation effect are focused [23,46,62–64]. However, as real TBG systems are not chiral symmetric, the Euler bands and their ideal limit without chiral symmetry might be a more appropriate starting point to examine correlation effects.

Moreover, to observe the genuine properties of interacting ideal Euler bands distinct from interacting ideal Chern bands, finding proper material platforms hosting ideal Euler bands is crucial. Thorough examination of the many-body instability in interacting ideal Euler bands is an important problem which we leave for future study.

Acknowledgments. S.K. and B.-J.Y. were supported by the Institute for Basic Science in Korea (Grant No. IBS-R009-D1), Samsung Science and Technology Foundation under Project No. SSTF-BA2002-06, and National Research Foundation of Korea (NRF) grants funded by the government of Korea (MSIT) (Grants No. 2021R1A2C4002773 and No. NRF-2021R1A5A1032996).

[1] G. W. Winkler, A. A. Soluyanov, and M. Troyer, Smooth gauge and Wannier functions for topological band structures in arbitrary dimensions, Phys. Rev. B **93**, 035453 (2016).
[2] K. v. Klitzing, G. Dorda, and M. Pepper, New method for high-accuracy determination of the fine-structure constant based on quantized Hall resistance, Phys. Rev. Lett. **45**, 494 (1980).
[3] K. von Klitzing, The quantized Hall effect, Rev. Mod. Phys. **58**, 519 (1986).
[4] R. B. Laughlin, Quantized Hall conductivity in two dimensions, Phys. Rev. B **23**, 5632 (1981).
[5] D. J. Thouless, M. Kohmoto, M. P. Nightingale, and M. den Nijs, Quantized Hall conductance in a two-dimensional periodic potential, Phys. Rev. Lett. **49**, 405 (1982).
[6] J. E. Avron, R. Seiler, and B. Simon, Homotopy and quantization in condensed matter physics, Phys. Rev. Lett. **51**, 51 (1983).
[7] J. E. Avron, L. Sadun, J. Segert, and B. Simon, Chern numbers, quaternions, and Berry's phases in Fermi systems, Commun. Math. Phys. **124**, 595 (1989).
[8] Y. Hatsugai, Chern number and edge states in the integer quantum Hall effect, Phys. Rev. Lett. **71**, 3697 (1993).
[9] Y. Hatsugai, Edge states in the integer quantum Hall effect and the Riemann surface of the Bloch function, Phys. Rev. B **48**, 11851 (1993).
[10] Y.-Q. Ma, Euler characteristic number of the energy band and the reason for its non-integer values, arXiv:2001.05946.
[11] Y.-Q. Ma, S.-J. Gu, S. Chen, H. Fan, and W.-M. Liu, The Euler number of Bloch states manifold and the quantum phases in gapped fermionic systems, Europhys. Lett. **103**, 10008 (2013).
[12] S. Peotta and P. Törmä, Superfluidity in topologically nontrivial flat bands, Nat. Commun. **6**, 8944 (2015).
[13] A. Julku, S. Peotta, T. I. Vanhala, D.-H. Kim, and P. Törmä, Geometric origin of superfluidity in the Lieb-lattice flat band, Phys. Rev. Lett. **117**, 045303 (2016).
[14] L. Liang, T. I. Vanhala, S. Peotta, T. Siro, A. Harju, and P. Törmä, Band geometry, Berry curvature, and superfluid weight, Phys. Rev. B **95**, 024515 (2017).
[15] T. Ozawa and B. Mera, Relations between topology and the quantum metric for Chern insulators, Phys. Rev. B **104**, 045103 (2021).
[16] C.-K. Chiu, J. C. Y. Teo, A. P. Schnyder, and S. Ryu, Classification of topological quantum matter with symmetries, Rev. Mod. Phys. **88**, 035005 (2016).
[17] C. L. Kane and E. J. Mele, Z_2 topological order and the quantum spin Hall effect, Phys. Rev. Lett. **95**, 146802 (2005).
[18] C. L. Kane and E. J. Mele, Quantum spin Hall effect in graphene, Phys. Rev. Lett. **95**, 226801 (2005).
[19] B. A. Bernevig and S.-C. Zhang, Quantum spin Hall effect, Phys. Rev. Lett. **96**, 106802 (2006).
[20] S. A. Parameswaran, R. Roy, and S. L. Sondhi, Fractional quantum Hall physics in topological flat bands, C. R. Phys. **14**, 816 (2013).
[21] M. Claassen, C. H. Lee, R. Thomale, X.-L. Qi, and T. P. Devereaux, Position-momentum duality and fractional quantum Hall effect in Chern insulators, Phys. Rev. Lett. **114**, 236802 (2015).
[22] C. H. Lee, M. Claassen, and R. Thomale, Band structure engineering of ideal fractional Chern insulators, Phys. Rev. B **96**, 165150 (2017).

[23] P. J. Ledwith, G. Tarnopolsky, E. Khalaf, and A. Vishwanath, Fractional Chern insulator states in twisted bilayer graphene: An analytical approach, Phys. Rev. Res. **2**, 023237 (2020).

[24] J. Ahn, S. Park, and B.-J. Yang, Failure of Nielsen-Ninomiya theorem and fragile topology in two-dimensional systems with space-time inversion symmetry: Application to twisted bilayer graphene at magic angle, Phys. Rev. X **9**, 021013 (2019).

[25] J. Ahn, D. Kim, Y. Kim, and B.-J. Yang, Band topology and linking structure of nodal line semimetals with Z_2 monopole charges, Phys. Rev. Lett. **121**, 106403 (2018).

[26] A. Bouhon, T. Bzdušek, and R.-J. Slager, Geometric approach to fragile topology beyond symmetry indicators, Phys. Rev. B **102**, 115135 (2020).

[27] A. Bouhon, Q. Wu, R.-J. Slager, H. Weng, O. V. Yazyev, and T. Bzdušek, Non-Abelian reciprocal braiding of Weyl points and its manifestation in ZrTe, Nat. Phys. **16**, 1137 (2020).

[28] Y. X. Zhao and Y. Lu, PT-symmetric real Dirac fermions and semimetals, Phys. Rev. Lett. **118**, 056401 (2017).

[29] P. Törmä, S. Peotta, and B. A. Bernevig, Superconductivity, superfluidity and quantum geometry in twisted multilayer systems, Nat. Rev. Phys. **4**, 528 (2022).

[30] F. Xie, Z. Song, B. Lian, and B. A. Bernevig, Topology-bounded superfluid weight in twisted bilayer graphene, Phys. Rev. Lett. **124**, 167002 (2020).

[31] K. Zhang, Y. Zhang, L. Fu, and E.-A. Kim, Fractional correlated insulating states at one-third filled magic angle twisted bilayer graphene, Commun. Phys. **5**, 250 (2022).

[32] T. Löthman, J. Schmidt, F. Parhizgar, and A. M. Black-Schaffer, Nematic superconductivity in magic-angle twisted bilayer graphene from atomistic modeling, Commun. Phys. **5**, 92 (2022).

[33] A. Julku, T. J. Peltonen, L. Liang, T. T. Heikkilä, and P. Törmä, Superfluid weight and Berezinskii-Kosterlitz-Thouless transition temperature of twisted bilayer graphene, Phys. Rev. B **101**, 060505(R) (2020).

[34] X. Hu, T. Hyart, D. I. Pikulin, and E. Rossi, Geometric and conventional contribution to the superfluid weight in twisted bilayer graphene, Phys. Rev. Lett. **123**, 237002 (2019).

[35] Y.-Q. Ma, S. Chen, H. Fan, and W.-M. Liu, Abelian and non-Abelian quantum geometric tensor, Phys. Rev. B **81**, 245129 (2010).

[36] A. T. Rezakhani, D. F. Abasto, D. A. Lidar, and P. Zanardi, Intrinsic geometry of quantum adiabatic evolution and quantum phase transitions, Phys. Rev. A **82**, 012321 (2010).

[37] D. Gonzalez, D. Gutiérrez-Ruiz, and J. D. Vergara, Phase space formulation of the Abelian and non-Abelian quantum geometric tensor, J. Phys. A: Math. Theor. **53**, 505305 (2020).

[38] G. Palumbo, Non-Abelian tensor Berry connections in multi-band topological systems, Phys. Rev. Lett. **126**, 246801 (2021).

[39] A. Zhang, Revealing Chern number from quantum metric, Chin. Phys. B **31**, 040201 (2022).

[40] M. Kolodrubetz, D. Sels, P. Mehta, and A. Polkovnikov, Geometry and non-adiabatic response in quantum and classical systems, Phys. Rep. **697**, 1 (2017).

[41] J. P. Provost and G. Vallee, Riemannian structure on manifolds of quantum states, Commun. Math. Phys. **76**, 289 (1980).

[42] B. Hetényi and P. Lévay, Fluctuations, uncertainty relations, and the geometry of quantum state manifolds, Phys. Rev. A **108**, 032218 (2023).

[43] R. Roy, Band geometry of fractional topological insulators, Phys. Rev. B **90**, 165139 (2014).

[44] S. A. Parameswaran, R. Roy, and S. L. Sondhi, Fractional Chern insulators and the W_∞ algebra, Phys. Rev. B **85**, 241308(R) (2012).

[45] T. S. Jackson, G. Möller, and R. Roy, Geometric stability of topological lattice phases, Nat. Commun. **6**, 8629 (2015).

[46] J. Wang, J. Cano, A. J. Millis, Z. Liu, and B. Yang, Exact Landau level description of geometry and interaction in a flatband, Phys. Rev. Lett. **127**, 246403 (2021).

[47] See Supplemental Material at http://link.aps.org/supplemental/10.1103/PhysRevB.109.L161111 for the details of the proof for Eq. (7); various characteristics of the band Euler insulator; the ideal condition for the Euler insulator; the influence of symmetry constraints on the relation between quantum geometry and topology; the calculational details for TBG model, which includes Refs. [65,66].

[48] G. Tarnopolsky, A. J. Kruchkov, and A. Vishwanath, Origin of magic angles in twisted bilayer graphene, Phys. Rev. Lett. **122**, 106405 (2019).

[49] B. Mera and T. Ozawa, Kähler geometry and Chern insulators: Relations between topology and the quantum metric, Phys. Rev. B **104**, 045104 (2021).

[50] S. M. Girvin, A. H. MacDonald, and P. M. Platzman, Collective-excitation gap in the fractional quantum Hall effect, Phys. Rev. Lett. **54**, 581 (1985).

[51] S. M. Girvin, A. H. MacDonald, and P. M. Platzman, Magneto-roton theory of collective excitations in the fractional quantum Hall effect, Phys. Rev. B **33**, 2481 (1986).

[52] A. Bouhon, A. Timmel, and R.-J. Slager, Quantum geometry beyond projective single bands, arXiv:2303.02180.

[53] W. J. Jankowski, A. S. Morris, A. Bouhon, F. Nur Ünal, and R.-J. Slager, Optical manifestations of topological Euler class in electronic materials, arXiv:2311.07545.

[54] H. C. Po, H. Watanabe, and A. Vishwanath, Fragile topology and Wannier obstructions, Phys. Rev. Lett. **121**, 126402 (2018).

[55] Y. Hwang, J. Ahn, and B.-J. Yang, Fragile topology protected by inversion symmetry: Diagnosis, bulk-boundary correspondence, and Wilson loop, Phys. Rev. B **100**, 205126 (2019).

[56] A. Bouhon, A. M. Black-Schaffer, and R.-J. Slager, Wilson loop approach to fragile topology of split elementary band representations and topological crystalline insulators with time-reversal symmetry, Phys. Rev. B **100**, 195135 (2019).

[57] B. Bradlyn, Z. Wang, J. Cano, and B. A. Bernevig, Disconnected elementary band representations, fragile topology, and Wilson loops as topological indices: An example on the triangular lattice, Phys. Rev. B **99**, 045140 (2019).

[58] Z.-D. Song, L. Elcoro, Y.-F. Xu, N. Regnault, and B. A. Bernevig, Fragile phases as affine monoids: Classification and material examples, Phys. Rev. X **10**, 031001 (2020).

[59] S. H. Kooi, G. van Miert, and C. Ortix, Classification of crystalline insulators without symmetry indicators: Atomic and fragile topological phases in twofold rotation symmetric systems, Phys. Rev. B **100**, 115160 (2019).

[60] S. Yang, Z.-C. Gu, K. Sun, and S. Das Sarma, Topological flat band models with arbitrary Chern numbers, Phys. Rev. B **86**, 241112(R) (2012).

[61] R. Bistritzer and A. H. MacDonald, Moiré bands in twisted double-layer graphene, Proc. Natl. Acad. Sci. USA **108**, 12233 (2011).

[62] J. Wang and Z. Liu, Hierarchy of ideal flatbands in chiral twisted multilayer graphene models, Phys. Rev. Lett. **128**, 176403 (2022).

[63] J. Wang, S. Klevtsov, and Z. Liu, Origin of model fractional Chern insulators in all topological ideal flatbands: Explicit color-entangled wave function and exact density algebra, Phys. Rev. Res. **5**, 023167 (2023).

[64] P. J. Ledwith, A. Vishwanath, and E. Khalaf, Family of ideal Chern flatbands with arbitrary Chern number in chiral twisted graphene multilayers, Phys. Rev. Lett. **128**, 176404 (2022).

[65] S. Chen, A. Bouhon, R.-J. Slager, and B. Monserrat, Non-Abelian braiding of Weyl nodes via symmetry-constrained phase transitions, Phys. Rev. B **105**, L081117 (2022).

[66] A. Tiwari and T. Bzdušek, Non-Abelian topology of nodal-line rings in $\mathcal{PT}$-symmetric systems, Phys. Rev. B **101**, 195130 (2020).